frontiers in Chemistry

ORIGINAL RESEARCH
published: 28 May 2021
doi: 10.3389/fchem.2021.681313

Humidity-Insensitive NO_2 Sensors Based on SnO_2/rGO Composites

Yingyi Wang[1,2], Lin Liu[2], Fuqin Sun[2,3], Tie Li[2,3], Ting Zhang[2,3]* and Sujie Qin[1]**

[1]Department of Health and Environmental Sciences, Xi'an Jiaotong-Liverpool University, Suzhou, China, [2]I-Lab, Key Laboratory of Multifunctional Nanomaterials and Smart Systems, Suzhou Institute of Nano-Tech and Nano-Bionics (SINANO), Chinese Academy of Sciences (CAS), Suzhou, China, [3]School of Nano-Tech and Nano-Bionics, University of Science and Technology of China, Hefei, China

This study reported a novel humidity-insensitive nitrogen dioxide (NO_2) gas sensor based on tin dioxide (SnO_2)/reduced graphene oxide (rGO) composites through the sol-gel method. The sensor demonstrated ppb-level NO_2 detection in p-type sensing behaviors (13.6% response to 750 ppb). Because of the synergistic effect on SnO_2/rGO p-n heterojunction, the sensing performance was greatly enhanced compared to that of bare rGO. The limit of detection of sensors was as low as 6.7 ppb under dry air. Moreover, benefited from the formed superhydrophobic structure of the SnO_2/rGO composites (contact angle: 149.0°), the humidity showed a negligible influence on the dynamic response (S_g) of the sensor to different concentration of NO_2 when increasing the relative humidity (RH) from 0 to 70% at 116°C. The relative conductivity of the sensor to 83% relative humidity was 0.11%. In addition, the response ratio (S_g/S_{RH}) between 750 ppb NO_2 and 83% RH was 649.0, indicating the negligible impaction of high-level ambient humidity on the sensor. The as-fabricated humidity-insensitive gas sensor can promise NO_2 detection in real-world applications such as safety alarm, chemical engineering, and so on.

Keywords: gas sensor, SnO_2/rGO composites, humidity-insensitive, low temperature, nitrogen dioxide (NO_2)

OPEN ACCESS

Edited by:
Jae-Hong Lim,
Gachon University, South Korea

Reviewed by:
Xingxing Gu,
Chongqing Technology and Business University, China
Yong-Ho Choa,
Hanyang University, South Korea

****Correspondence:***
Tie Li
Tli2014@sinano.ac.cn
Ting Zhang
Tzhang2009@sinano.ac.cn
Sujie Qin
Sujie.Qin@xjtlu.edu.cn

Specialty section:
This article was submitted to Nanoscience, a section of the journal Frontiers in Chemistry

Received: *16 March 2021*
Accepted: *10 May 2021*
Published: *28 May 2021*

Citation:
Wang Y, Liu L, Sun F, Li T, Zhang T and Qin S (2021) Humidity-Insensitive NO_2 Sensors Based on SnO_2/rGO Composites. Front. Chem. 9:681313. doi: 10.3389/fchem.2021.681313

INTRODUCTION

Air pollution has become a pressing global issue facing the development of industry and technology. Nitrogen dioxide (NO_2), as one of the most toxic air pollutants, is generated from industries and vehicle emissions, which can cause some serious environmental issues such as haze, photochemical smog, and acid rain (Mallik and Lal, 2014). United Statess Occupational Safety and Health Administration (OSHA) reported that when the concentration of NO_2 is over 1 ppm, inhalation of NO_2 for 15 min will cause some respiratory diseases such as asthma (Cheng, et al., 2019; Yuvaraja, et al., 2020). In the urban atmosphere, the concentration of NO_2 commonly measured in the range from 20 to 100 ppb (Brunet, et al., 2008). Therefore, a NO_2 sensor, which is sensitive enough to detect at least 20 ppb or ultralow concentration of NO_2 (ppb level), is urgently demanded.

Up to now, metal oxide semiconductors-based NO_2 sensors have been used in many applications owing to high chemical stability and low cost of sensing materials such as CuO (Bo, et al., 2020; Wang Y, et al., 2020), ZnO (Wang J, et al., 2019; Choi, et al., 2020), WO_3 (Liu, et al., 2020; Wang M, et al., 2020), NiO (Wei, et al., 2019; Wilson, et al., 2020), and SnO_2 (Kamble, et al., 2017; Zhong, et al., 2019). Among them, SnO_2 is a typical n-type wide bandgap semiconductor (3.6 eV) that has been regarded as one of the most promising industrialized candidates for NO_2 sensing due to its attractive characteristics, including controlled size, low limits of detection, and facile large-scale fabrication (Maeng, et al., 2014; Lee, et al., 2015). However, there are several shortcomings of pure SnO_2-based

sensors that limit their practical applications. Firstly, aggregation occurs when the size is too small during the material synthesis and the sensor fabrication processes, which decreases the surface-specific area, reduces the sensitivity of gas sensors and influences the long-term stability of the as-fabricated sensor (Li, et al., 2015; Wu, et al., 2020). Meanwhile, the SnO_2-based gas sensor generally needs a high operation temperature (>200°C) to achieve high sensitivity, which causes high power consumption (Van Hieu, 2010; Guo J, et al., 2016). Nowadays, combining SnO_2 with low-dimensional materials (e.g., MoS_2 (Qiao, et al., 2018), carbon nanotube (Minh Nguyet, et al., 2017), metal oxide (Park, et al., 2020), graphene (Hu, et al., 2020), etc.) to form p-n heterojunction has been regarded as the prospective strategies to overcome the shortcomings of pure SnO_2-based gas sensors (Yin, et al., 2014; Gui, et al., 2018). Among low-dimensional materials, owing to the low-cost, ultrahigh specific surface area, controllable bandgap and various oxygen-containing functional group (e.g., C-O, O-C=O, and O-C(O)-O), rGO is an ideal material to obtain high-performance gas sensor by decorating with metal oxides (Guo, et al., 2019; Yin, et al., 2020). Hence, constructing p-n heterojunction between rGO and SnO_2 is a potential approach to enhance the sensing performance of sensors through modulating the carrier transportation due to different working functions (Neri, et al., 2013; Choi, et al., 2014; Kim, et al., 2018). For example, Zhu, et al. (2017) reported a NO_2 gas sensor based on rGO/SnO_2 nanocomposites, and the sensing response of sensors increased three times compared with that of sensors based on pure rGO. Meanwhile, Kim, et al. (2017) fabricated graphene-SnO_2 nanocomposites (SnO_2-G)-based sensors, and the sensing response of SnO_2-G-based sensors toward 1 ppm NO_2 is 24.7, which is around two folds higher than that of SnO_2-based sensors. Similarly, Lin, et al. (2020) prepared Co_3O_4/N-doped rGO (N-rGO) nanocomposites-based ethanol sensors. The sensing response value of Co_3O_4/N-rGO-based sensors to 100 ppm ethanol at 200°C is around 20 folds higher than that of N-rGO-based sensors.

Although heterojunction enhances the gas sensing performance, the high-level nonconstant humidity will severely impact the sensing performances of these reported NO_2 sensors, which is difficult to distinguish the target gas from ambient humidity and hinder the applications in the real world. For example, Wang, et al. (2018) fabricated Pd-SnO_2-RGO-based NO_2 sensors and showed 76% sensing response to 1 ppm NO_2 gas. However, when the sensor exposed to NO_2 gas with 80% RH, the sensing response declined by 20%. The limit of detection of Pd-SnO_2-RGO-based NO_2 sensors is 50 ppb under dry air. Similarly, Guo, et al. (2019) reported Bi@rGO/SnO_2-based benzene sensors. The sensing response to 5 ppm benzene with 60% RH is three times lower than that without humidity. Degler, et al. (2018) found that the gas sensing response cannot be controlled by doping different noble metal content (Pt) on SnO_2. To date, there are some strategies have been developed to address this issue, including the construction of gas preconcentration techniques and dehumidification techniques (Groves and Zellers, 2001; Peng, et al., 2008). However, these methods are costly, complex, and sacrifice the sensor's sensitivity (Konvalina and Haick, 2012).

To solve these problems, we proposed the humidity-insensitive NO_2 sensors based on SnO_2/rGO p-n heterojunction, which was used to detect NO_2 at low temperatures (as low as 116°C). The sensing performance of SnO_2/rGO composite-based NO_2 sensors was studied, and the LOD was found to be as low as 6.7 ppb, which is below the standard of United States OSHA and NO_2 pollutant concentration in the urban atmosphere. Notably, the NO_2 sensor showed a reliable sensing response under increasing relative humidity conditions (3–70% RH), and the resistance of the sensor almost kept constant under 83% RH, promising real-world applications.

MATERIALS AND METHODS

Materials and Synthesis of Composites

Natural graphite flake (325 meshes, 99.8%) was purchased from Sigma Aldrich; H_2SO_4 (AR) and $KMnO_4$ (AR) was purchased from Shanghai Hushi Laboratorial Equipment Co., Ltd.; $SnCl_4.5H_2O$ (AR) was purchased from Macklin; Epichlorohydrin (PPD) (Analytical reagent) and N, N-Dimethylformamide (DMF) (97%) were purchased from Aladdin. These reagents were used without any further purification. The micro-hotplates were purchased from Leanstar-Tech Co., Ltd. The SnO_2/rGO composite was prepared through a sol-gel method. Briefly, the GO was synthesized from nature graphite powder based on modified Hummer's method. Secondly, the $SnCl_4{\cdot}5H_2O$ and epichlorohydrin (PPD) were slowly added into the GO/DMF solution and stirred for a short time. The SnO_2/rGO composite was formed after three days of solution exchange and dried by supercritical CO_2 to carbonize at 600°C for 2 h under the Ar atmosphere. The synthesized sensing material was suspended in a dimethylformamide solution (DMF) solution. The SnO_2/rGO composite was drop-coated onto the micro-hotplate to fabricate gas sensors. After that, sensors were annealed at 200°C for 20 min under Ar atmosphere protection to reduce the contacting barrier.

Characterization of Composites and Microstructures

The morphology and crystal structure of SnO_2/rGO composites were analyzed by scanning electron microscopy (SEM, Hitachi-s4800), transmission electron microscopy (TEM, Tecnai G2 F20 S-Twin). The chemical composite of materials was carried out by energy dispersive spectrometry (EDS, FEI, Quanta FEG 250). The crystal lattice was analyzed by X-ray Diffraction (XRD, Bruker AXS, D8 Advance). The degree of reduction of rGO was characterized by Raman spectroscopy (Raman, Horriba-JY, LABRAM HR).

Measurements Sensing Performance of NO_2 Sensors

The gas sensing performance under dry air (~3% RH) was investigated by a designed testing system based on previous work (Liu, et al., 2019). In general, firstly, the sensor chip was

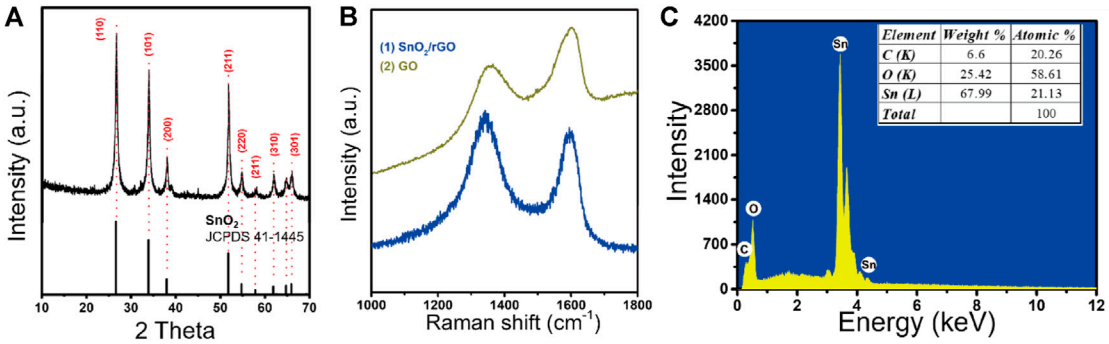

FIGURE 1 | (A) The XRD patterns of SnO_2/rGO composites; **(B)** the Raman spectra of SnO_2/rGO composites and GO; **(C)** the EDS analysis of SnO_2/rGO composites.

connected in series with a loaded resistor, which was selected to close to sensor resistance to optimize the resolution obtained from measurements. Secondly, the specific concentration of NO_2, which was implemented by dry air (80% N_2 and 20% O_2) and controlled by mass flow controllers (MFCs, Sevenstar CS200, China), goes through a quartz chamber (volume: 1 cm^3, 200 sccm). Finally, sensor resistance was determined by the Fieldpoint analog input and output modules by continuously controlling and monitoring the voltage of the circuit (National Instruments, Austin, TX). The loaded resistor calculated by Ohm's law was recorded in a custom LabView computer program (**Supplementary Figure S1**).

Measurements Sensing Performance of NO_2 Sensors Under Humidity

Dynamic conductivity response to high humidity conditions (83% RH) was tested by the KNO_3 saturated saline solution, added to a humidity controller (**Supplementary Figure S1**). Saturated saline solutions produce various saturated vapor pressures and form different relative humidity (Greenspan, 1977). One commercial high-precision temperature/humidity sensor (Sensirion Company, SHT75) was used as the reference sensor to detect real-time humidity. The static relative response to various concentrations of NO_2 under 70% RH was tested in the homemade testing chamber (20 L) (**Supplementary Figure S2**). The specific high concentration of NO_2 gas was injected into the testing chamber and diluted by the air in the testing chamber. The air humidity (~70% RH) of the day is recorded as the ambient humidity.

RESULTS AND DISCUSSION

Material Characterizations

The crystal structure of SnO_2/rGO composites was examined by XRD, as shown in **Figure 1A**. The positions of characteristic peaks are located at 2θ = 26.61°, 33.89°, 37.95°, 51.78°, 54.76°, 64.72°, and 65.94°, which are, respectively, collaborated with (110), (101), (200), (211), (220), (310), and (301) planes of tetragonal rutile SnO_2 (JCPDS. 41–1,445). Compared with the reported XRD patterns of pristine rGO at 2θ = 24.7° and 42.8° (Wang Z, et al., 2019), SnO_2/rGO composites do not show a peak assigned to rGO. The high density of SnO_2 nanoparticles is uniformly decorated on the surface of the rGO, which can prevent the reassembled behavior of SnO_2 and cover its XRD pattern information (Zhang, et al., 2014). Moreover, the Raman spectroscopy was employed to further study the reduced structure of the rGO in SnO_2/rGO composites (**Figure 1B**). The peaks located at around 1,341 and 1,594 cm^{-1} are assigned to the typical D band and G band of rGO, respectively, (Guo D, et al., 2016). The intensity ratio of D peak to G peak (I_D/I_G) of SnO_2/rGO (1.12) is higher than that of GO (0.81), which indicates that the oxygen functional groups (e.g., C-O, O-C=O, and O-C(O)-O) have been removed and induced defects during the synthesis process (Tuan, et al., 2018; Hu, et al., 2017; Xu, et al., 2019). The EDS analysis (**Figure 1C**) shows that the product contained C, O, Sn elements. The atomic ratios of Sn, O, and C are 21.13, 58.61, and 20.26%, respectively. These results indicate that no other impurities and crystals were mixed in the reaction product.

The morphology of SnO_2/rGO composites was characterized via the SEM and TEM techniques and displayed in **Figure 2**. It can be seen from **Figure 2A,B** that the SnO_2 nanoparticles (NPs) are uniformly and densely anchored on the surfaces of the rGO nanosheets without any agglomeration. The low-resolution TEM images in **Figure 2C** show the size distribution of the SnO_2 NPs in the composites, around 5.5 nm with normal distribution from 4.5 to 6.5 nm (**Figure 2C**, inset). Moreover, the high-resolution TEM (HRTEM) image of SnO_2/rGO in **Figure 2D** shows that the SnO_2 NPs are highly crystallized with a crystalline interplanar spacing of ~0.335 nm, which is attributed to the (110) crystal plane.

Gas Sensing Performances

The gas sensing performance of the SnO_2/rGO composite-based sensors was tested. The relative responses of the sensors were defined as the relative changes of resistance in the air and those in target gases: $S_g = (|R_g - R_a|/R_a)*100\%$ for oxidizing gas or $S_g = (|R_a - R_g|/R_a)*100\%$ for reducing gas (where R_a is the sensor resistance in air and R_g is the sensor resistance in target gas). **Figure 3A** shows the response of these sensors to 1.5 ppm of

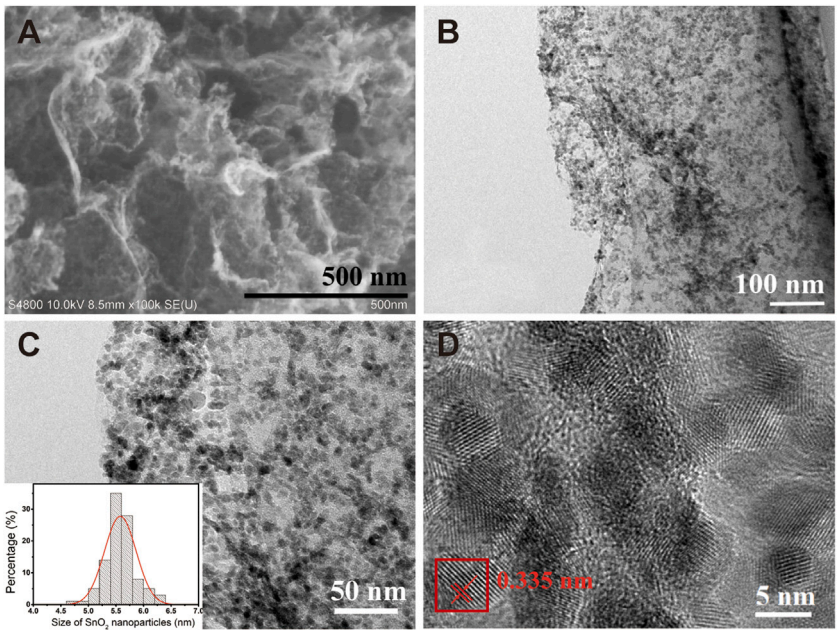

FIGURE 2 | (A) Typical SEM images of SnO_2/rGO composites; **(B, C)** Low magnification TEM images of SnO_2/rGO composites, (c, inset) SnO_2 NPs size distribution histogram; **(D)** the HRTEM image and corresponding crystalline interplanar of SnO_2/rGO composites.

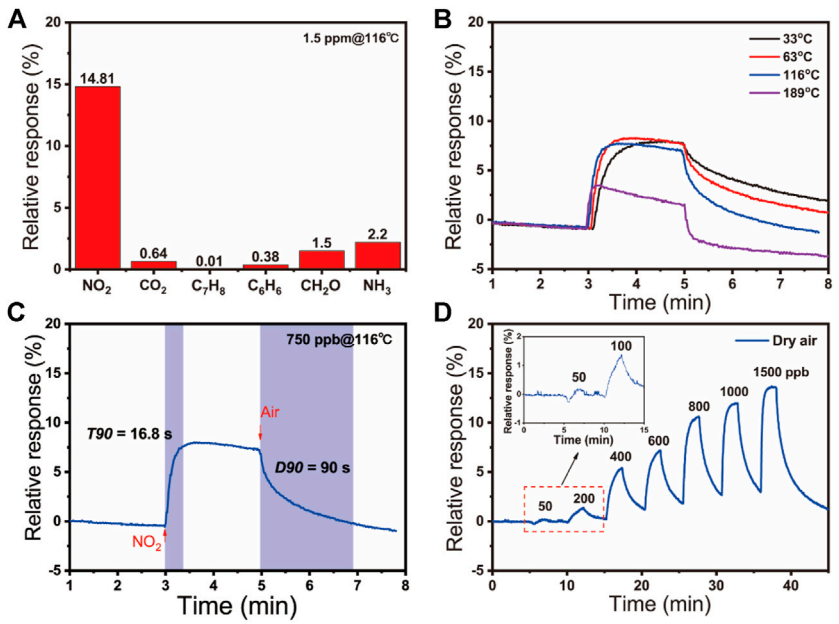

FIGURE 3 | (A) The relative responses of SnO_2/rGO composite-based sensors to different gases (NO_2, CO_2, C_7H_8, C_6H_6, CH_2O, and NH_3) at 116°C; **(B)** The response curves to 750 ppb NO_2 at the increasing operating temperature of 33, 63, 116, 189°C; **(C)** The response curve to 750 ppb NO_2 of sensors based on SnO_2/rGO composites at 116°C; **(D)** The relative responses to different concentrations of NO_2 (50–1500 ppb) under dry air.

various gases at 116°C, including ammonia (NH_3), methanal (CH_2O), benzene (C_6H_6), toluene (C_7H_8), carbon dioxide (CO_2), and NO_2. The result reveals that the as-prepared SnO_2/rGO composite has high selectivity to NO_2 compared with other gases. It attributed to the relatively high adsorption energy of NO_2 on sensing materials among these gases (Huang, et al., 2008; Schröder, 2013; Lazar, et al., 2013; Chakradhar, et al., 2016; Zhu, et al., 2021), indicating its high selectivity to NO_2 (**Supplementary Table S1**). To determine the optimized operating temperature, **Figure 3B** and **Supplementary Table S1**

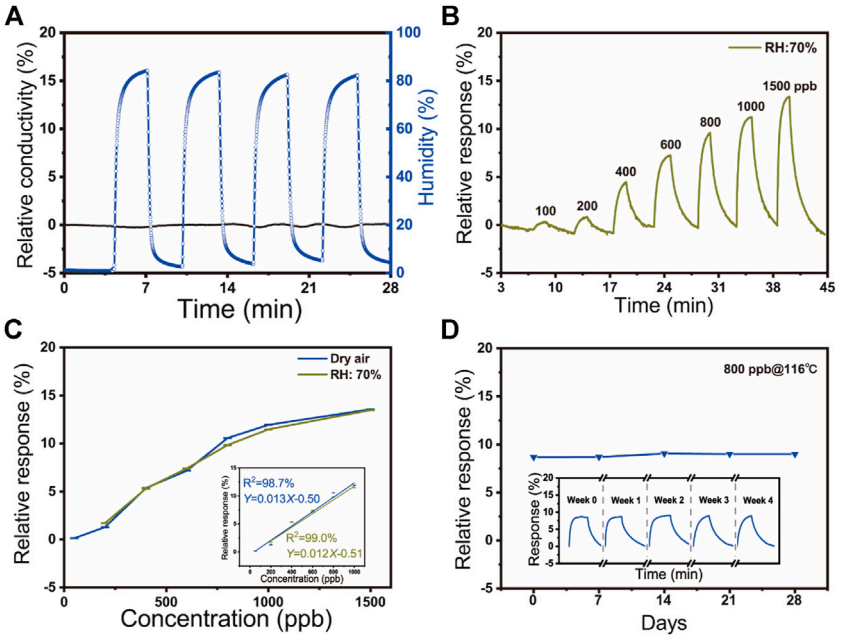

FIGURE 4 | (A) The relative response of sensors in high humidity in four cycles (83% RH); **(B)** The relative response to different concentrations of NO_2 (50–1500 ppb) under 70% RH environment at 116°C; **(C)** The relative response of the various NO_2 concentration to ambient humidity at 116°C; (c. inset) The linear fit between the concentration of NO_2 and dynamic response under dry air (blue) and 70% RH (green) at 116°C; **(D)** Long time stability of SnO_2/rGO composite-based sensors to 800 ppb NO_2 at room temperature for about 28 days; (d. inset) The repeatability of sensors to 800 ppb NO_2 during the five testing cycles at 116°C.

show the response plots of SnO_2/rGO composite-based NO_2 sensors toward 750 ppb NO_2 at the serial operation temperature from 33 to 189°C. The relative response of sensors at low temperature (e.g., 33, 63, and 116°C) have slight difference (7.80% at 33°C, 8.29% at 63°C, and 7.57% at 116°C) and then it dramatically decreased by further increasing the operation temperature (3.51% at 189°C). However, the response time (T90) and recovery time (D90) dramatically decrease along with the operating temperature increase. The T90 and D90 are, respectively, defined as the time required for a sensor to reach 90% of the stable resistance value when the test gas is turned on and off. As **Figure 3C** shows, the fast T90 (7 s) and D90 (31 s) of NO_2 sensors to 750 ppb NO_2 are obtained when the operating temperature was elevating to 189°C. Decreasing the operating temperature to 116°C, the T90 and D90 of NO_2 sensors increase to 17 and 90 s, respectively, (**Figure 3C**; **Supplementary Figure S3**). When the devices worked at 63 and 33°C, the T90 and D90 have been further increased (**Supplementary Figure S4**; **Supplementary Table S2**). Because of the similar and relatively high response value at 33, 63, and 116°C, SnO_2/rGO composite-based sensors are regarded as the candidate to work at room temperature. The temperature can affect the adsorption/desorption process on the sensing materials and sensor surface. The rate of adsorption/desorption increases as the temperature rose, resulting in a shorter T90 and D90 (Walker, et al., 2019). However, when the temperature arrives too high, the quantity and properties of active sites on the surface of sensing materials have been changed (Neri, et al., 2013), which causes the adsorbed oxygen species and NO_2 cannot remain on the surface of sensing materials to undergo a reaction (Jinkawa, et al., 2000), resulting in a low sensing response and the drifting of baseline were observed correspondently. Therefore, taking the T90, D90, and the relative response of NO_2 sensors into consideration, the optimal operating temperature was chosen to be 116°C. **Figure 3D** demonstrates the dynamic response of sensors to various NO_2 concentrations at dry air from 50 to 1,500 ppb, indicating a broad response range. Contrastively, the sensing performances of pure rGO to 4 ppm were dramatically declined (**Supplementary Figure S5**), which attracted the electrons from rGO to SnO_2 and enhanced sensing performance by SnO_2/rGO composite-based NO_2 sensors.

The dynamic responses of SnO_2/rGO composite-based NO_2 sensors toward high humidity (around 83% RH) have been measured (**Figure 4A**). It can be seen that the relative conductivity of NO_2 sensors shows extremely weak fluctuation (~0.11%). Compared with other works and the commercial bare NO_2 sensor (MEMS NO_2 sensor, GM-102B, Zhenzhou Winsen Electronics Technology Co., Ltd.) summarized in **Supplementary Table S3**, as-fabricated SnO_2/rGO composite-based NO_2 sensors showed an extremely high response ratio (S_g/S_{RH} = 649.0) between 750 ppb NO_2 and 83% RH, which indicates that the high-level ambient humidity shows negligible impaction on the NO_2 sensor. Moreover, the static sensing performance of the sensor to different concentrations of NO_2 (from 200 to 1,500 ppb) under the real-world environment (70% RH) was estimated (**Figure 4B**). Compared with the above-obtained results under dry air, as **Figure 4C** showed, the two curves have similar trends and the effect of humidity on the sensor can be neglected. The

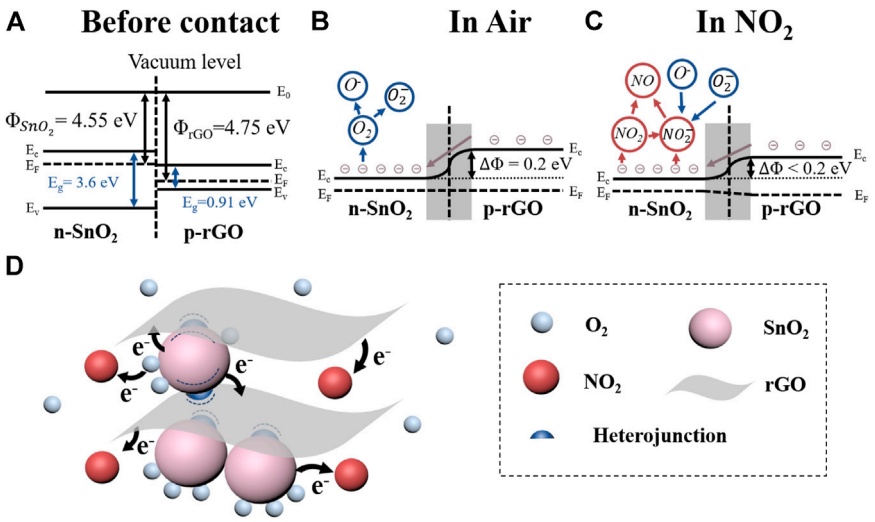

FIGURE 5 | (A) Schematic bandgap structure of n-type SnO_2 and p-type rGO; **(B)** Schematic bandgap structure of SnO_2/rGO heterojunction in air and **(C)** in NO_2; **(D)** Schematic of sensing mechanisms of SnO_2/rGO composite-based sensors with exposure to NO_2.

humidity-insensitive property of high-performance NO_2 sensors attributes to the formed superhydrophobic structure of SnO_2/rGO composites, which the exhibited contact angle is 149.0° (**Supplementary Figure S6**). Two main factors determine the superhydrophobicity of a material surface: surface roughness and surface energy. In general, a rough surface with low surface energy leads to a hydrophobic surface (Lin, et al., 2011; Chen and Dong, 2013). The as-fabricated SnO_2/rGO composites by this sol-gel method have high porosity and high surface roughness (Lin, et al., 2011). Meanwhile, the high anneal temperature (600°C) during carbonized process vastly decreases the hydrophilic oxygen-containing function groups on the rGO surface (e.g., C-O, O-C=O, and O-C(O)-O), which can decrease the surface energy of SnO_2/rGO composites and form a superhydrophobic surface (Wu, et al., 2018; Xu, et al., 2019; Cao, et al., 2019). The performance of humidity insensitivity of the NO_2 sensor may be weakened by working temperature (116°C) in some extent. However, the superhydrophobic structure of nanocomposites plays a vital role in the humidity insensitivity of the NO_2 sensor (Phan and Chung, 2015; Wu, et al., 2018).

The relative response of the sensor increased along with the increase of the concentration of the NO_2 whatever under humid air or not (50–1,500 ppb under dry air and 200–1,500 ppb under 70% RH) (**Figure 4C**). Meanwhile, it can be observed that the relative response exhibits a rapidly increasing linear trend under the low concentration of 1,000 ppb, indicating that SnO_2/rGO composite-based sensors have an excellent sensing performance for the detection of low-concentration NO_2. The observed slope differences between the low concentration (below 1,000 ppb) and the high concentration (1,500 ppb) could be attributed to the degradation of electron transfer and saturation phenomenon of the SnO_2/rGO composites under high NO_2 concentration. The linear fit of the gas response of the sensor to the various concentration of NO_2 can be represented by relative response = b Concentration + a. The inset of **Figure 4C** indicates that the SnO_2/rGO composite-based NO_2 sensors have a linear correlation (R^2 > 98%). According to linear fit results, the theoretical limit of detection (LOD) of NO_2 under 0 and 70% RH are calculated as 6.7 and 25 ppb based on **Eq. 1**, respectively, (Mateos, et al., 2019; Song, et al., 2016). Both LODs are below the threshold concentration for causing diseases and the NO_2 pollutant concentration in the urban atmosphere.

$$LOD = 3 \times \frac{RMS_{noise}}{Slope} \quad (1)$$

RMS_{noise} is the standard deviation of the noise level. Under dry air, the RMS_{noise} (0.029) was obtained from 150 baseline data points before exposure to NO_2 from **Figure 3D**. Thus, according to **Figure 5A** (inset), the LOD was around 6.7 ppb. Under 70% RH, the RMS_{noise} (0.10) was obtained from 150 data. And the calculated LOD was about 25 ppb. **Figure 4D** illustrated the long-time stability of SnO_2/rGO composite-based sensors to 800 ppb NO_2 at room temperature for 28 days. The response is maintained between 8 and 9% and the standard deviation of NO_2 sensors is 0.19, which indicated its good stability of sensitivity. However, the T90 and D10 varies as a function of deterioration of time which implies the sensor (**Figure 4D** inset).

Sensing Mechanism

The sensing performance of SnO_2/rGO composite-based sensors to NO_2 shows a p-type sensing behavior indicating that the rGO dominates the conduction channel of NO_2 sensors. In the vacuum state, the working functions of SnO_2 ($\Phi_{(SnO2)}$) and rGO ($\Phi_{(rGO)}$) are 4.55 and 4.75 eV, respectively, (Kim, et al., 2016) (**Figure 5A**). As **Figure 5B** showed, after connection, the electrons will be transferred from SnO_2 to rGO at the hetero-interface to balance the Fermi level (E_f). Because of the charge transfer, it will form a depletion layer and heterojunction potential barrier ($\Delta\Phi_{hetero}$ = 0.2 eV). In the

air, oxygen molecules will adsorb on the surface of SnO_2/rGO composites and withdraw electrons from SnO_2 to form O_2^- and O^-. Since the diameter of SnO_2 nanoparticles is comparable or less than two times the Debye length (λ_D ~6 nm) of the SnO_2 in the air, the SnO_2 nanoparticles will almost fully deplete after adsorption of oxygen molecules (Xu, et al., 1991) (**Figure 5B**). Once exposed to NO_2, owing to the high electron affinity of NO_2 molecules, the NO_2 molecules will further withdraw the electrons from oxygen ions and SnO_2/rGO composites, as shown in **Eqs. 2–5** and **Figure 5C**.

$$NO_2 + e^- \rightarrow NO_2^- \quad (2)$$

$$NO_2 + e^- \rightarrow NO + O^- \quad (3)$$

$$2NO_2 + O_2^- + e^- \rightarrow 2NO_2^- + O_2 \quad (4)$$

$$NO_2^- + O^- + 2e^- \rightarrow NO + 2O^{2-} \quad (5)$$

The Fermi level of SnO_2 will shift far away from the conduction band leading to the reduction of the $\Delta\Phi_{hetero}$. Meanwhile, the hole accumulation layer will form at the surface of rGO in the air and forma homojunction potential barrier ($\Delta\Phi_{homo}$). When exposing to NO_2, the NO_2 molecules can directly adsorb on the surface of rGO and withdraw the electrons from rGO, which leads to an increasing in the hole concentration and reduction of the $\Delta\Phi_{homo}$ (Miller, et al., 2014). As the resistance of sensors based on heterogeneous materials is exponential with the changing of the effective potential barrier ($\Delta\Phi$, including $\Delta\Phi_{hetero}$ and $\Delta\Phi_{homo}$, according to **Eq. 6** (Feng, et al., 2017; Hua, et al., 2017). Thus, due to the synergistic effect of the $\Delta\Phi_{hetero}$ and $\Delta\Phi_{homo}$, the sensing performance of SnO_2/rGO composites is greatly improved compared with bare rGO (**Supplementary Figure S3**).

$$R = R_0 \exp\left(\frac{\Delta\Phi}{k_b T}\right) \quad (6)$$

where R_0 is constant, k_b is Boltzmann's constant, T is the absolute temperature, and $\Delta\Phi$ is the effective potential barrier (including homojunction barrier and heterojunction barrier).

CONCLUSION

In summary, this work demonstrated the simple sol-gel method to decorate rGO nanosheet with SnO_2 NPs to improve NO_2 detection. Due to the synergistic effect of SnO_2/rGO p-n heterojunction and rGO/rGO homojunction, the sensing performance of SnO_2/rGO composites was greatly enhanced compared with that of bare rGO. A low LOD of 6.7 ppb was obtained at 116°C under dry air. Compared with the reported humidity-insensitive NO_2 sensors, the designed SnO_2/rGO composite-based NO_2 sensor showed an extremely high response ratio (649.0) between 750 ppb NO_2 and 83% RH. The superhydrophobic property of the fabricated SnO_2/rGO composites contributes to the humidity insensitivity. The superhydrophobic property is caused by the high roughness and low surface energy of the SnO_2/rGO composites. It is promised to use the SnO_2/rGO composite-based NO_2 sensors in real-world applications.

DATA AVAILABILITY STATEMENT

The original contributions presented in the study are included in the article/**Supplementary Material**, further inquiries can be directed to the corresponding authors.

AUTHOR CONTRIBUTIONS

YW and LL contributed equally to this work.

All authors listed have made a substantial, direct, and intellectual contribution to the work and approved it for publication.

FUNDING

The authors acknowledge the funding support from the National Key R&D Program of China (2017YFA0701101, 2020YFB2008501), the National Natural Science Foundation of China (51702354, 62071462), the Youth Promotion Association of Chinese Academy of Sciences (2020320), the Foundation Research Project of Jiangsu Province (BK20201195), and the Suzhou Key Industrial Technology Innovation Project (SYG202029).

SUPPLEMENTARY MATERIAL

The Supplementary Material for this article can be found online at: https://www.frontiersin.org/articles/10.3389/fchem.2021.681313/full#supplementary-material

REFERENCES

Bo, Z., Wei, X., Guo, X., Yang, H., Mao, S., Yan, J., et al. (2020). SnO_2 Nanoparticles Incorporated CuO Nanopetals on Graphene for High-Performance Room-Temperature NO_2 Sensor. *Chemical Physics Letters.* 750, 137485. doi:10.1016/j.cplett.2020.137485

Brunet, J., Garcia, V. P., Pauly, A., Varenne, C., and Lauron, B. (2008). An Optimised Gas Sensor Microsystem for Accurate and Real-Time Measurement of Nitrogen Dioxide at Ppb Level. *Sensors Actuators B: Chem.* 134, 632–639. doi:10.1016/j.snb.2008.06.010

Cao, Y., Zhao, Y., Wang, Y., Zhang, Y., Wen, J., Zhao, Z., et al. (2019). Reduction Degree Regulated Room-Temperature Terahertz Direct Detection Based on Fully Suspended and Low-Temperature Thermally Reduced Graphene Oxides. *Carbon* 144, 193–201. doi:10.1016/j.carbon.2018.12.023

Chakradhar, A., Sivapragasam, N., Nayakasinghe, M. T., and Burghaus, U. (2016). Adsorption Kinetics of Benzene on Graphene: An Ultrahigh Vacuum Study. *J. Vacuum Sci. Techn. A: Vacuum, Surf. Films.* 34, 021402. doi:10.1116/1.4936337

Chen, Z., Dong, L., Yang, D., and Lu, H. (2013). Yang D and Lu HSuperhydrophobic Graphene-Based Materials: Surface Construction and Functional Applications. *Adv. Mater.* 25, 5352–5359. doi:10.1002/adma.201302804

Cheng, M., Wu, Z., Liu, G., Zhao, L., Gao, Y., Zhang, B., et al. (2019). Highly Sensitive Sensors Based on quasi-2D rGO/SnS2 Hybrid for Rapid Detection of NO2 Gas. *Sensors Actuators B: Chem.* 291, 216–225. doi:10.1016/j.snb.2019.04.074

Choi, H., Kwon, S., Lee, W., Im, K., Kim, T., Noh, B., et al. (2020). Ultraviolet Photoactivated Room Temperature NO_2 Gas Sensor of ZnO Hemitubes and Nanotubes Covered with TiO_2 Nanoparticles. *Nanomater.* 10, 462. doi:10.3390/nano10030462

Choi, S.-W., Katoch, A., Kim, J.-H., and Kim, S. S. (2014). Prominent Reducing Gas-Sensing Performances of N-SnO2 Nanowires by Local Creation of P-N Heterojunctions by Functionalization with P-Cr2O3 Nanoparticles. *ACS Appl. Mater. Inter.* 6, 17723–17729. doi:10.1021/am504164j

Degler, D., Müller, S. A., Doronkin, D. E., Wang, D., Grunwaldt, J.-D., Weimar, U., et al. (2018). Platinum Loaded Tin Dioxide: A Model System for Unravelling the Interplay between Heterogeneous Catalysis and Gas Sensing. *J. Mater. Chem. A.* 6, 2034–2046. doi:10.1039/C7TA08781K

Feng, Q., Li, X., and Wang, J. (2017). Percolation Effect of Reduced Graphene Oxide (rGO) on Ammonia Sensing of rGO-SnO2 Composite Based Sensor. *Sensors Actuators B: Chem.* 243, 1115–1126. doi:10.1016/j.snb.2016.12.075

Greenspan, L. (1977). Humidity Fixed Points of Binary Saturated Aqueous Solutions. *J. Res. Natl. Bur. Stan. Sect. A.* 81A, 89. doi:10.6028/jres.081A.011

Groves, W., and Zellers, E. (2001). Analysis of Solvent Vapors in Breath and Ambient Air with a Surface Acoustic Wave Sensor Array. *Ann. Occup. Hyg.* 45, 609–623. doi:10.1093/annhyg/45.8.60910.1016/s0003-4878(01)00020-5

Gui, Y.-h., Wang, H.-y., Tian, K., Yang, L.-l., Guo, H.-s., Zhang, H.-z., et al. (2018). Enhanced Gas Sensing Properties to NO2 of SnO2/rGO Nanocomposites Synthesized by Microwave-Assisted Gas-Liquid Interfacial Method. *Ceramics Int.* 44, 4900–4907. doi:10.1016/j.ceramint.2017.12.080

Guo, D., Cai, P., Sun, J., He, W., Wu, X., Zhang, T., et al. (2016). Reduced-graphene-oxide/metal-oxide P-N Heterojunction Aerogels as Efficient 3d Sensing Frameworks for Phenol Detection. *Carbon* 99, 571–578. doi:10.1016/j.carbon.2015.12.074

Guo, J., Zhang, J., Gong, H., Ju, D., and Cao, B. (2016). Au Nanoparticle-Functionalized 3D SnO2 Microstructures for High Performance Gas Sensor. *Sensors Actuators B: Chem.* 226, 266–272. doi:10.1016/j.snb.2015.11.140

Guo, W., Zhou, Q., Zhang, J., Fu, M., Radacsi, N., and Li, Y. (2019). Hydrothermal Synthesis of Bi-doped SnO2/rGO Nanocomposites and the Enhanced Gas Sensing Performance to Benzene. *Sensors Actuators B: Chem.* 299, 126959. doi:10.1016/j.snb.2019.126959

Hu, J., Chen, M., Rong, Q., Zhang, Y., Wang, H., Zhang, D., et al. (2020). Formaldehyde Sensing Performance of Reduced Graphene Oxide-Wrapped Hollow SnO2 Nanospheres Composites. *Sensors Actuators B: Chem.* 307, 127584. doi:10.1016/j.snb.2019.127584

Hu, R., Zhao, J., and Zheng, J. (2017). Synthesis of SnO 2/rGO Hybrid Materials by Sol-Gel/thermal Reduction Method and its Application in Electrochemical Capacitors. *Mater. Lett.* 197, 59–62. doi:10.1016/j.matlet.2017.03.082

Hua, Z., Qiu, Z., Li, Y., Zeng, Y., Wu, Y., Tian, X., et al. (2017). A Theoretical Investigation of the Power-Law Response of Metal Oxide Semiconductor Gas Sensors II: Size and Shape Effects. Sensors & Actuators B:. *Chemical* 255, 3541–3549. doi:10.1016/j.snb.2017.09.189

Huang, B., Li, Z., Liu, Z., Zhou, G., Hao, S., Wu, J., et al. (2008). Adsorption of Gas Molecules on Graphene Nanoribbons and its Implication for Nanoscale Molecule Sensor. *J. Phys. Chem. C* 112, 13442–13446. doi:10.1021/jp8021024

Jinkawa, T., Sakai, G., Tamaki, J., Miura, N., and Yamazoe, N. (2000). Relationship between Ethanol Gas Sensitivity and Surface Catalytic Property of Tin Oxide Sensors Modified with Acidic or Basic Oxides. *J. Mol. Catal. A: Chem.* 155, 193–200. doi:10.1016/S1381-1169(99)00334-9

Kamble, D. L., Harale, N. S., Patil, V. L., Patil, P. S., and Kadam, L. D. (2017). Characterization and NO2 Gas Sensing Properties of spray Pyrolyzed SnO2 Thin Films. *J. Anal. Appl. Pyrolysis* 127, 38–46. doi:10.1016/j.jaap.2017.09.004

Kim, H. W., Na, H. G., Kwon, Y. J., Kang, S. Y., Choi, M. S., Bang, J. H., et al. (2017). Microwave-Assisted Synthesis of Graphene-SnO2 Nanocomposites and Their Applications in Gas Sensors. *ACS Appl. Mater. Inter.* 9, 31667–31682. doi:10.1021/acsami.7b02533

Kim, J.-H., Lee, J.-H., Mirzaei, A., Kim, H. W., and Kim, S. S. (2018). SnO2 (N)-NiO (P) Composite Nanowebs: Gas Sensing Properties and Sensing Mechanisms. *Sensors Actuators B: Chem.* 258, 204–214. doi:10.1016/j.snb.2017.11.063

Kim, J. H., Katoch, A., Kim, H. W., and Sang, S. K. (2016). Realization of ppm-level co detection with an exceptionally high sensitivity using reduced graphene oxide-loaded SnO_2 nanofibers with the au functionalization. *Chem Commun.* 52, 3832. doi:10.1039/C5CC10482C

Konvalina, G., and Haick, H. (2012). Effect of Humidity on Nanoparticle-Based Chemiresistors: A Comparison between Synthetic and Real-World Samples. *ACS Appl. Mater. Inter.* 4, 317–325. doi:10.1021/am2013695

Lazar, P., Karlický, F., Jurečka, P., Kocman, M., Otyepková, E., Šafářová, K., et al. (2013). Adsorption of Small Organic Molecules on Graphene. *J. Am. Chem. Soc.* 135, 6372–6377. doi:10.1021/ja403162r

Lee, J.-H., Katoch, A., Choi, S.-W., Kim, J.-H., Kim, H. W., and Kim, S. S. (2015). Extraordinary Improvement of Gas-Sensing Performances in SnO2 Nanofibers Due to Creation of Local P-N Heterojunctions by Loading Reduced Graphene Oxide Nanosheets. *ACS Appl. Mater. Inter.* 7, 3101–3109. doi:10.1021/am5071656

Li, L., He, S., Liu, M., Zhang, C., and Chen, W. (2015). Three-Dimensional Mesoporous Graphene Aerogel-Supported SnO2 Nanocrystals for High-Performance NO2 Gas Sensing at Low Temperature. *Anal. Chem.* 87, 1638–1645. doi:10.1021/ac503234e

Lin, G., Wang, H., Lai, X., Yang, R., Zou, Y., Wan, J., et al. (2020). Co3O4/N-Doped RGO Nanocomposites Derived from MOFs and Their Highly Enhanced Gas Sensing Performance. *Sensors Actuators B: Chem.* 303, 127219. doi:10.1016/j.snb.2019.127219

Lin, Y., Ehlert, G. J., Bukowsky, C., and Sodano, H. A. (2011). Superhydrophobic Functionalized Graphene Aerogels. *ACS Appl. Mater. Inter.* 3, 2200–2203. doi:10.1021/am200527j

Liu, H., Xu, Y., Zhang, X., Zhao, W., Ming, A., and Wei, F. (2020). Enhanced NO2 Sensing Properties of Pt/WO3 Films Grown by Glancing Angle Deposition. *Ceramics Int.* 46, 21388–21394. doi:10.1016/j.ceramint.2020.05.236

Liu, L., Wang, Y., Dai, Y., Li, G., Wang, S., Li, T., et al. (2019). *In Situ* Growth of NiO@SnO2 Hierarchical Nanostructures for High Performance H2S Sensing. *ACS Appl. Mater. Inter.* 11, 44829–44836. doi:10.1021/acsami.9b13001

Maeng, S., Kim, S.-W., Lee, D.-H., Moon, S.-E., Kim, K.-C., and Maiti, A. (2014). SnO2 Nanoslab as NO2 Sensor: Identification of the NO2 Sensing Mechanism on a SnO2 Surface. *ACS Appl. Mater. Inter.* 6, 357–363. doi:10.1021/am404397f

Mallik, C., and Lal, S. (2014). Seasonal Characteristics of SO2, NO2, and CO Emissions in and Around the Indo-Gangetic Plain. *Environ. Monit. Assess.* 186, 1295–1310. doi:10.1007/s10661-013-3458-y

Mateos, M., Tchangaï, M.-D., Meunier-Prest, R., Heintz, O., Herbst, F., Suisse, J.-M., et al. (2019). Low Conductive Electrodeposited Poly(2,5-Dimethoxyaniline) as a Key Material in a Double Lateral Heterojunction, for Sub-ppm Ammonia Sensing in Humid Atmosphere. *ACS Sens.* 4, 740–747. doi:10.1021/acssensors.9b00109

Miller, D. R., Akbar, S. A., and Morris, P. A. (2014). Nanoscale Metal Oxide-Based Heterojunctions for Gas Sensing: A Review. *Sensors Actuators B: Chem.* 204, 250–272. doi:10.1016/j.snb.2014.07.074

Minh Nguyet, Q. T., Van Duy, N., Phuong, N. T., Trung, N. N., Hung, C. M., Hoa, N. D., et al. (2017). Superior Enhancement of NO2 Gas Response Using N-P-N Transition of Carbon nanotubes/SnO2 Nanowires Heterojunctions. *Sensors Actuators B: Chem.* 238, 1120–1127. doi:10.1016/j.snb.2016.07.143

Neri, G., Leonardi, S. G., Latino, M., Donato, N., Baek, S., Conte, D. E., et al. (2013). Sensing Behavior of SnO2/reduced Graphene Oxide Nanocomposites toward NO2. *Sensors Actuators B: Chem.* 179, 61–68. doi:10.1016/j.snb.2012.10.031

Park, K.-R., Cho, H.-B., Lee, J., Song, Y., Kim, W.-B., and Choa, Y.-H. (2020). Design of Highly Porous SnO2-CuO Nanotubes for Enhancing H2S Gas Sensor Performance. *Sensors Actuators B: Chem.* 302, 127179. doi:10.1016/j.snb.2019.127179

Peng, G., Trock, E., and Haick, H. (2008). Detecting Simulated Patterns of Lung Cancer Biomarkers by Random Network of Single-Walled Carbon Nanotubes Coated with Nonpolymeric Organic Materials. *Nano Lett.* 8, 3631–3635. doi:10.1021/nl801577u

Phan, D.-T., and Chung, G.-S. (2015). Effects of Rapid thermal Annealing on Humidity Sensor Based on Graphene Oxide Thin Films. *Sensors Actuators B: Chem.* 220, 1050–1055. doi:10.1016/j.snb.2015.06.055

Qiao, X.-Q., Zhang, Z.-W., Hou, D.-F., Li, D.-S., Liu, Y., Lan, Y.-Q., et al. (2018). Tunable MoS2/SnO2 P-N Heterojunctions for an Efficient Trimethylamine Gas Sensor and 4-Nitrophenol Reduction Catalyst. *ACS Sustainable Chem. Eng.* 6, 12375–12384. doi:10.1021/acssuschemeng.8b02842

Schröder, E. (2013). Methanol Adsorption on Graphene. *J. Nanomater.* 2013, 1–6. doi:10.1155/2013/871706

Song, Z., Wei, Z., Wang, B., Luo, Z., Xu, S., Zhang, W., et al. (2016). Sensitive Room-Temperature H2S Gas Sensors Employing SnO2 Quantum Wire/Reduced Graphene Oxide Nanocomposites. *Chem. Mater.* 28, 1205–1212. doi:10.1021/acs.chemmater.5b04850

Tuan, P. V., Hieu, L. T., Ngoc, T. K., Hoang, C., Hoa, N. D., Hoa, T. T. Q., et al. (2018). Hydrothermal Synthesis, Structure, and Photocatalytic Properties of SnO_2/rgo Nanocomposites with Different Go Concentrations. *Materials Research Express* 5, 095506. doi:10.1088/2053-1591/aad6ca

Van Hieu, N. (2010). Comparative Study of Gas Sensor Performance of SnO_2 Nanowires and Their Hierarchical Nanostructures. Sensors and Actuators B: *Chemical* 150, 112–119. doi:10.1016/j.snb.2010.07.033

Walker, J. M., Akbar, S. A., and Morris, P. A. (2019). Synergistic Effects in Gas Sensing Semiconducting Oxide Nano-Heterostructures: A Review. *Sensors Actuators B: Chem.* 286, 624–640. doi:10.1016/j.snb.2019.01.049

Wang, J., Shen, Y., Li, X., Xia, Y., and Yang, C. (2019). Synergistic Effects of UV Activation and Surface Oxygen Vacancies on the Room-Temperature NO2 Gas Sensing Performance of ZnO Nanowires. *Sensors Actuators B: Chem.* 298, 126858. doi:10.1016/j.snb.2019.126858

Wang, Z., Jia, Z., Li, Q., Zhang, X., Sun, W., Sun, J., et al. (2019). The Enhanced NO2 Sensing Properties of SnO2 Nanoparticles/reduced Graphene Oxide Composite. *J. Colloid Interf. Sci.* 537, 228–237. doi:10.1016/j.jcis.2018.11.009

Wang, M., Wang, Y., Li, X., Ge, C., Hussain, S., Liu, G., et al. (2020). WO3 Porous Nanosheet Arrays with Enhanced Low Temperature NO2 Gas Sensing Performance. *Sensors Actuators B: Chem.* 316, 128050. doi:10.1016/j.snb.2020.128050

Wang, Y., Xue, J., Zhang, X., Si, J., Liu, Y., Ma, L., et al. (2020). Novel Intercalated CuO/black Phosphorus Nanocomposites: Fabrication, Characterization and NO_2 Gas Sensing at Room Temperature. *Mater. Sci. Semiconductor Process.* 110, 104961. doi:10.1016/j.mssp.2020.104961

Wang, Z., Han, T., Fei, T., Liu, S., and Zhang, T. (2018). Investigation of Microstructure Effect on NO2 Sensors Based on SnO2 Nanoparticles/Reduced Graphene Oxide Hybrids. *ACS Appl. Mater. Inter.* 10, 41773–41783. doi:10.1021/acsami.8b15284

Wei, Z., Zhou, Q., Wang, J., Lu, Z., Xu, L., and Zeng, W. (2019). Hydrothermal Synthesis of SnO2 Nanoneedle-Anchored NiO Microsphere and its Gas Sensing Performances. *Nanomaterials* 9, 1015. doi:10.3390/nano9071015

Wilson, R. L., Simion, C. E., Stanoiu, A., Taylor, A., Guldin, S., Covington, J. A., et al. (2020). Humidity-tolerant Ultrathin Nio Gas-Sensing Films. *ACS Sens.* 5, 1389–1397. doi:10.1021/acssensors.0c00172

Wu, J., Li, Z., Xie, X., Tao, K., Liu, C., Khor, K. A., et al. (2018). 3D Superhydrophobic Reduced Graphene Oxide for Activated NO2 Sensing with Enhanced Immunity to Humidity. *J. Mater. Chem. A.* 6, 478–488. doi:10.1039/c7ta08775f

Wu, J., Wu, Z., Ding, H., Wei, Y., Huang, W., Yang, X., et al. (2020). Three-Dimensional Graphene Hydrogel Decorated with SnO2 for High-Performance NO2 Sensing with Enhanced Immunity to Humidity. *ACS Appl. Mater. Inter.* 12, 2634–2643. doi:10.1021/acsami.9b18098

Xu, C., Tamaki, J., Miura, N., and Yamazoe, N. (1991). Grain Size Effects on Gas Sensitivity of Porous SnO2-Based Elements. *Sensors Actuators B: Chem.* 3, 147–155. doi:10.1016/0925-4005(91)80207-z

Xu, D., Liu, J., Chen, P., Yu, Q., Wang, J., Yang, S., et al. (2019). *In Situ* growth and Pyrolysis Synthesis of Super-hydrophobic Graphene Aerogels Embedded with Ultrafine β-Co Nanocrystals for Microwave Absorption. *J. Mater. Chem. C* 7, 3869–3880. doi:10.1039/C9TC00294D

Yin, F., Li, Y., Yue, W., Gao, S., Zhang, C., and Chen, Z. (2020). Sn3O4/rGO Heterostructure as a Material for Formaldehyde Gas Sensor with a Wide Detecting Range and Low Operating Temperature. *Sensors Actuators B: Chem.* 312, 127954. doi:10.1016/j.snb.2020.127954

Yin, L., Chen, D., Cui, X., Ge, L., Yang, J., Yu, L., et al. (2014). Normal-pressure Microwave Rapid Synthesis of Hierarchical SnO2@rGO Nanostructures with Superhigh Surface Areas as High-Quality Gas-Sensing and Electrochemical Active Materials. *Nanoscale* 6, 13690–13700. doi:10.1039/C4NR04374J

Yuvaraja, S., Surya, S. G., Chernikova, V., Vijjapu, M. T., Shekhah, O., Bhatt, P. M., et al. (2020). Realization of an Ultrasensitive and Highly Selective OFET NO2 Sensor: The Synergistic Combination of PDVT-10 Polymer and Porphyrin-MOF. *ACS Appl. Mater. Inter.* 12, 18748–18760. doi:10.1021/acsami.0c00803

Zhang, H., Feng, J., Fei, T., Liu, S., and Zhang, T. (2014). SnO2 Nanoparticles-Reduced Graphene Oxide Nanocomposites for NO2 Sensing at Low Operating Temperature. *Sensors Actuators B: Chem.* 190, 472–478. doi:10.1016/j.snb.2013.08.067

Zhong, Y., Li, W., Zhao, X., Jiang, X., Lin, S., Zhen, Z., et al. (2019). High-Response Room-Temperature NO2 Sensor and Ultrafast Humidity Sensor Based on SnO2 with Rich Oxygen Vacancy. *ACS Appl. Mater. Inter.* 11, 13441–13449. doi:10.1021/acsami.9b01737

Zhu, X., Guo, Y., Ren, H., Gao, C., and Zhou, Y. (2017). Enhancing the NO2 Gas Sensing Properties of rGO/SnO2 Nanocomposite Films by Using Microporous Substrates. *Sensors Actuators B: Chem.* 248, 560–570. doi:10.1016/j.snb.2017.04.030

Zhu, X., Xu, Y., Cheng, Z., Wang, Y., Lu, Z., and Zhang, G. (2021). First Principles Study of Atmospheric Pollutants Adsorption on Non-defect and Monatomic Defect Graphene. *Diamond Relat. Mater.* 112, 108252. doi:10.1016/j.diamond.2021.108252

Conflict of Interest: The authors declare that the research was conducted in the absence of any commercial or financial relationships that could be construed as a potential conflict of interest.